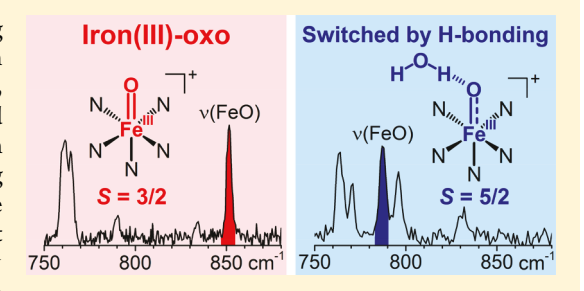
Trapping Iron(III)—Oxo Species at the Boundary of the "Oxo Wall": Insights into the Nature of the Fe(III)-O Bond

Erik Andris,^{†,⊥} Rafael Navrátil,^{†,⊥} Juraj Jašík,[†] Mayank Puri,[‡] Miquel Costas,*^{,§} Lawrence Que, Jr.,*^{,‡} and Jana Roithová*,^{†,|}

Supporting Information

ABSTRACT: Terminal non-heme iron(IV)—oxo compounds are among the most powerful and best studied oxidants of strong C-H bonds. In contrast to the increasing number of such complexes (>80 thus far), corresponding one-electron-reduced derivatives are much rarer and presumably less stable, and only two iron(III)-oxo complexes have been characterized to date, both of which are stabilized by hydrogen-bonding interactions. Herein we have employed gas-phase techniques to generate and identify a series of terminal iron(III)-oxo complexes, all without built-in hydrogen bonding. Some of these complexes exhibit ~70 cm⁻¹ decrease in $\nu(\text{Fe-O})$ frequencies expected for a half-order decrease in



bond order upon one-electron reduction to an S = 5/2 center, while others have $\nu(\text{Fe-O})$ frequencies essentially unchanged from those of their parent iron(IV)-oxo complexes. The latter result suggests that the added electron does not occupy a d orbital with Fe=O antibonding character, requiring an S = 3/2 spin assignment for the nascent Fe^{III}–O⁻ species. In the latter cases, water is found to hydrogen bond to the Fe^{III}–O⁻ unit, resulting in a change from quartet to sextet spin state. Reactivity studies also demonstrate the extraordinary basicity of these iron(III)—oxo complexes. Our observations show that metal—oxo species at the boundary of the "Oxo Wall" are accessible, and the data provide a lead to detect iron(III)—oxo intermediates in biological and biomimetic reactions.

INTRODUCTION

In Nature, high-valent iron-oxo compounds are involved in the oxidation of unactivated C-H bonds in alkanes, transformations catalyzed by heme and non-heme ironcontaining oxygenases. 2-11 Inspired by these oxygenases, chemists have prepared and characterized synthetic iron-(IV)-oxo complexes, 12-15 which have been useful for interpreting enzymatic spectroscopic data and for performing detailed mechanistic studies of oxidation reactions. However, despite much effort, reproducing the oxidative efficiency of enzymes in C-H oxidations with synthetic complexes remains a key challenge. The oxidation of aliphatic C-H bonds is initiated by hydrogen atom transfer (HAT) from the substrate to the high-valent iron—oxo species.8 Thermochemically, HAT can be regarded as a combination of electron and proton transfers. 16 The electron transfer is driven by the electrophilicity of the active iron center, whereas the proton transfer depends on the basicity of the iron-oxo intermediate. Therefore, understanding one-electron reduction of iron-(IV)-oxo intermediates and characterizing the resulting iron(III)—oxo complexes may provide further insights into the

HAT mechanism. Moreover, iron(III)—oxo intermediates have been implicated in the electron transfer-proton transfer (ET-PT) mechanism proposed for reactions of iron(IV)-oxo complexes with electron-rich substrates, such as dimethylanilines. 21-24

Reports on mononuclear iron(III)-oxo complexes are exceedingly rare. Indeed, only two iron(III)-oxo complexes have been crystallographically characterized thus far: $[(H_3 \text{buea}) \text{Fe}^{\text{III}}(O)]^{2-}$, by the Borovik group, 25 and $[(N_3 \text{buea}) \text{Fe}^{\text{III}}(O)]^{2-}$ (afa^{Cy})₃)Fe^{III}(O)]⁺, by the Fout group.²⁶ Both of these highspin complexes employ second-sphere hydrogen-bond donors to stabilize the terminal oxo unit within the trigonal ligand framework.²⁷ Conversely, no tetragonal terminal iron(III)-oxo complexes have yet been structurally characterized, presumably due to their instability. The instability results from the occupation of antibonding orbitals in complexes with a delectron count of 5, leading to a π bond order of only 0.5 for a low-spin iron(III) center.²⁸ This phenomenon is more

Received: August 20, 2018 Published: October 10, 2018



Department of Organic Chemistry, Faculty of Science, Charles University, Hlavova 2030/8, 128 43 Prague 2, Czech Republic

^{*}Department of Chemistry and Center for Metals in Biocatalysis, University of Minnesota, Minneapolis, Minnesota 55455, United States

[§]Departament de Quimica and Institute of Computational Chemistry and Catalysis (IQCC), University of Girona, Campus Montilivi, Girona 17071, Spain

Institute for Molecules and Materials, Radboud University, Heyendaalseweg 135, 6525 AJ Nijmegen, Netherlands

Journal of the American Chemical Society

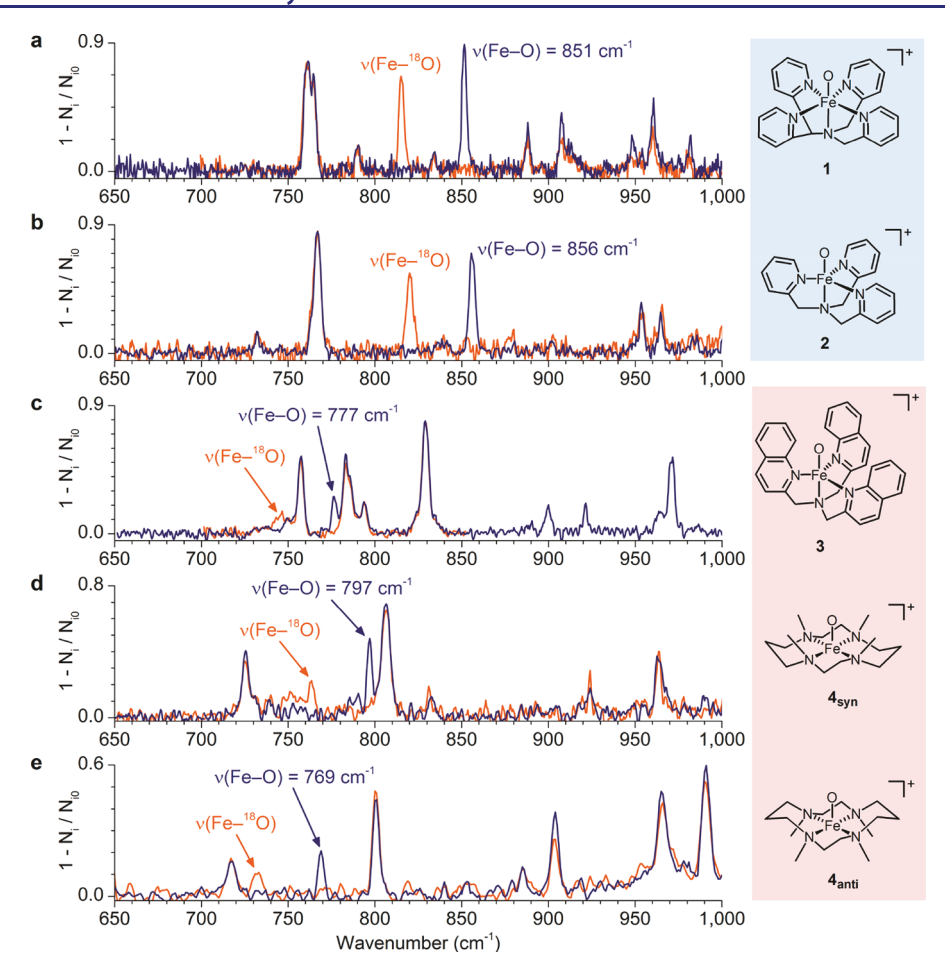


Figure 1. Infrared photodissociation spectra of terminal iron(III)—oxo complexes **1**–4 measured at 3 K. Blue and orange traces correspond to ¹⁶O and ¹⁸O labeling of the oxo ligand, respectively. The region between 700 and 850 cm⁻¹ in panel (d) was measured with twice longer irradiation time compared with the rest of the spectrum.

commonly referred to as the "Oxo Wall". $^{28-33}$ The formation of a tetragonal iron(III)—oxo complex by one-electron reduction of $[(TMC)Fe^{IV}(O)(CH_3CN)]^{2+}$ in dry acetonitrile has been proposed by Nam and Fukuzumi, but the postulated iron(III) product was not well characterized. 20 Thus, the effects from one-electron reduction of a tetragonal iron(IV)—oxo complex, in particular on its Fe—O vibrational frequency, remain unknown.

In this study, we report the gas-phase generation and characterization of the following terminal iron(III)-oxo complexes ($[(L)Fe^{III}(O)]^+$; Figure 1): $[(N4Py)Fe^{III}(O)]^+$ (1; N4Py = N,N-bis(2-pyridylmethyl)-N-bis(2-pyridyl)methylamine),³⁴ [(TPA)Fe^{III}(O)]⁺ (2; TPA = tris(2-pyridylmethyl)amine), 35 [(TQA)Fe^{III}(O)]⁺ (3; TQA = tris(2-quinolylmethyl)amine), 36 [(TMC)Fe^{III}(O_{syn})]⁺ (4_{syn}; TMC = 1,4,8,11-tetramethyl-1,4,8,11-tetraazacyclotetradecane; oxo atom syn to the four TMC methyl groups), and [(TMC)- $[Fe^{III}(O_{anti})]^+$ (4_{anti}; oxo atom *anti* to the four TMC methyl groups). 37,38 We have examined complexes 1–4 by heliumtagging infrared (IR) and visible (vis) photodissociation spectroscopy at 3 K, thus allowing us to determine for the first time the Fe-O vibrational frequencies and spin states of nonstabilized iron(III)-oxo compounds. We prepared the iron(III)-oxo complexes in the gas phase either by oneelectron reduction of $[(L)Fe^{IV}(O)]^{2+}$ complexes in collisions with tetrakis(dimethylamino)ethylene (TDAE) or by collisional activation and dissociation of the [(L)Fe^{II}(ONO₂)]⁺

precursors.^{39,40} The reactivity of these iron(III)—oxo complexes toward potential proton donor, hydrogen atom donor, and hydrogen bonding substrates has also been explored, in comparison with a prototypical iron(IV)—oxo analogue.

■ EXPERIMENTAL AND COMPUTATIONAL DETAILS

Preparation of lons. The iron(III)—oxo ions were formed from $[(L)Fe^{II}(NO_3)]^+$ precursor ions prepared by mixing a 1 mM acetonitrile solution of $[(L)Fe^{II}(OTf)_2]$ complex with 6 equiv of nitric acid. The precursor ions were transferred to the gas phase by electrospray ionization (see Figure S1a for typical ionization conditions). During the ionization process, the $[(L)Fe^{II}(NO_3)]^+$ ions lost the NO_2 radical and yielded the desired $[(L)Fe^{III}(O)]^+$ ions (eq 1). Similarly, the O-labeled $[(L)Fe^{III}(^{18}O)]^+$ ions were prepared using ^{18}O -labeled nitric acid.

$$[(L)Fe^{II}(NO_3)]^+ \rightarrow [(L)Fe^{III}(O)]^+ + NO_2$$
 (1)

Alternatively, the iron(III)—oxo ions 1 and 4_{anti} were prepared from the corresponding iron(IV)—oxo complexes by one-electron reduction in the gas phase. Specifically, we introduced gaseous TDAE at $\sim\!0.5$ Torr pressure in a 3 cm long collision cell mounted onto the transfer quadrupole in the electrospray ionization source. This led to the formation of iron(III)—oxo complexes along with the TDAE cation radical (eq 2 and Figure S1c).

$$[(L)Fe^{IV}(O)]^{2+} + TDAE \rightarrow [(L)Fe^{III}(O)]^{+} + TDAE^{+\bullet}$$
 (2)

Photodissociation Spectroscopy. The mass-selected [(L)Fe^{III}-(O)]⁺ ions were analyzed by photodissociation spectroscopy in the IR and vis spectral ranges using the ISORI instrument and the helium-

tagging method at 3 K. 42,43 Briefly, the mass-selected ions were guided into the ion trap and cooled to 3 K using a helium buffer gas. Under these conditions, vibrationally relaxed ions formed weakly bound complexes with helium atoms. Subsequently, the helium complexes were irradiated by a tunable IR/vis laser and, upon resonant absorption, the helium complexes dissociated. The IR/vis photodissociation (IRPD/visPD) spectra were acquired by recording the dissociation yield $(1 - N_i/N_{i0})$ while scanning the laser frequency. All presented spectra were recorded by monitoring the dissociation of the complexes with one helium tagging atom. The dissociation is a singlephoton process because the binding energy of a helium tagging atom is very low (below 0.1 kcal mol⁻¹). The effect of a helium tagging atom on the spectra is negligible, as previously discussed.44 further experimental details, please refer to Figures S1-S3. The visPD spectra (see Figure 3, below) were processed by dividing the measured attenuation by the laser energy (expressed as mJ·s; laser energy in Figure S3a). The intensity in the spectrum shown in Figure 4, below, was divided by the laser power (Figure S3b) to account for laser energy fluctuations. A wavelength meter WS-600 from HighFinesse GmbH was used for accurate determination of wavelength.

Complexes with Water. The ions, to some extent, also attach gaseous impurities (nitrogen, water) present in the helium buffer gas or in the instrument during the tagging process. By controlling the pulse sequence, we were able to generate a sufficient number of hydrated complexes $1 \cdot H_2O$, $2 \cdot H_2O$, and $3 \cdot H_2O$, which were subsequently tagged by a helium atom. Finally, IR or vis irradiation produced the helium-tagging IRPD or visPD spectra (see Figure 6, below, and Figure S8).

Gas-Phase Reactivity. Gas-phase reactivity was measured with a TSQ 7000 quadrupole-octopole-quadrupole tandem mass spectrometer. 45,46 The ions were mass-selected by the first quadrupole and guided into the octopole collision cell filled with a reactive gas at 0.2 mTorr pressure. The products were mass-analyzed by the second quadrupole. Relative reaction rates were measured at nominally zero collision energy from retarding potential analysis. Typical full width at half-maximum of the kinetic energy distribution of the ions was 1-1.2eV. The reported uncertainties correspond to the standard deviations from two measurements and do not include uncertainty in the measured pressure, which is 15% (the pressure was measured with 120 AA Baratron from MKS Instruments). Control experiments at zero pressure showed no significant signals besides that of the parent ion. Intermolecular kinetic isotope effects (KIEs) for reactions with ethanethiol were obtained from the competition experiments with EtSH/EtSD mixture. The EtSH/EtSD ratio in the collision cell was determined from a ligand exchange reaction with gold(I) complexes for which KIE = 1 was assumed. For further details, please refer to

Calculation Details. All calculations were performed with the B3LYP-D3 functional^{47–51} and 6-311+g** basis set using the Gaussian 09 package.⁵² All structures were fully optimized and confirmed as minima by diagonalization of the mass-weighted Hessian matrix. Wave functions of the doublet states have broken symmetry. Optimizations with the constrained symmetry led to unstable wave functions and energies about 1 kcal mol⁻¹ larger than the energies of the solutions with broken symmetry. XYZ coordinates are provided in the Supporting Information.

■ RESULTS AND DISCUSSION

The tetragonal complex $[(N4Py)Fe^{III}(O)]^+$ (1) features an Fe–O stretching vibration at 851 cm⁻¹ (815 cm⁻¹ with ¹⁸O labeling; Figure 1a and Figure S4). Surprisingly, this is only 2 cm⁻¹ lower than the Fe–O frequency of the corresponding iron(IV)—oxo complex $[(N4Py)Fe^{IV}(O)]^{2+}$ measured under similar conditions. ⁵³ The almost unchanged Fe–O frequency suggests that the electron occupancies of the d orbitals $(d_{xz}, d_{yz}, d_{yz}, d_{yz})$ involved in Fe–O antibonding are identical for 1 and its one-electron-oxidized Fe^{IV}(O) analogue. Therefore, the

only possible electronic configuration consistent with the results is the quartet state (Figure 2a, middle), in which the d

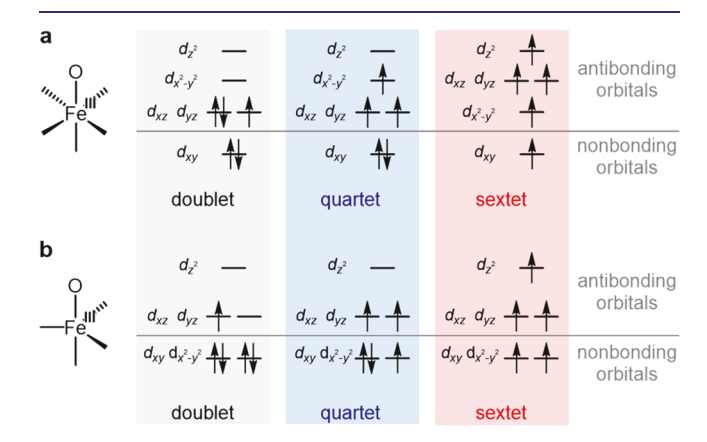


Figure 2. Possible electronic configurations of tetragonal (a) and trigonal (b) terminal iron(III)—oxo complexes. The reversed ordering between $\mathrm{d}_{x^2-y^2}$ and $\mathrm{d}_{xz}/\mathrm{d}_{yz}$ orbitals (a, sextet) results from our DFT calculations. The energy level diagram is simplified and does not show possible splitting due to low-symmetry ligand field components and spin—orbit coupling.

electron introduced must end up in the $d_{x^2-y^2}$ orbital. This assignment is further confirmed by the electronic absorption spectrum of 1 (Figure 3a), which displays an intense maximum at 450 nm and a broad band between 580 and 610 nm. The positions and intensities of the absorption bands agree with the theoretical spectrum of the quartet state predicted by timedependent density functional theory (TD-DFT) calculations (Figure 3f). According to the TD-DFT assignment, these transitions correspond to metal-to-ligand charge transfer (MLCT) from a doubly occupied d_{xy} orbital to π^* orbitals of pyridine rings (Figure S10a). The DFT calculations incorrectly predict the ground state of 1 as sextet, whereas the experimentally assigned quartet state is 0.8 kcal mol⁻¹ higher in energy, also based on DFT calculations. This discrepancy is not unexpected based on the limited accuracy of the DFT method.

Surprisingly, the Fe-O band of the trigonal complex $[(TPA)Fe^{III}(O)]^+$ (2) is located at 856 cm⁻¹ (820 cm⁻¹ with ¹⁸O labeling; Figure 1b and Figure S5), at a frequency quite similar to that of complex 1, despite the different denticity of their supporting ligands and consequent change to trigonal geometry for 2. The DFT calculations again suggest that the quartet and sextet states of 2 are almost isoenergetic, whereas the doublet spin state is much higher in energy and can be thus excluded. The sextet and quartet states of 2 have different theoretical vis absorption spectra, as shown in Figure 3g. The experimental spectrum shown in Figure 3b features an intense absorption band peaking at 450 nm and a shoulder at 500 nm, in agreement with the quartet spin state prediction (Figure 3g). Based on TD-DFT predictions, the observed bands correspond to MLCT transitions from a $d_{\pi \nu}$ orbital to π^* orbitals of the pyridine rings (Figure S10b). Additionally, we detected an electronic transition of 2 in the IR range (Figure 4). This is a broad absorption band ranging from 1650 to 4000 cm⁻¹ with a maximum around 2200 cm⁻¹ (4550 nm). According to TD-DFT calculations, this band is predicted at $4300~\text{cm}^{-1}$ (2300 nm) and corresponds to a spin-allowed d-d transition (Figure \$10c).⁵⁴ In addition, the spectrum contains IR absorptions of the TPA ligand, such as C=C stretching Journal of the American Chemical Society

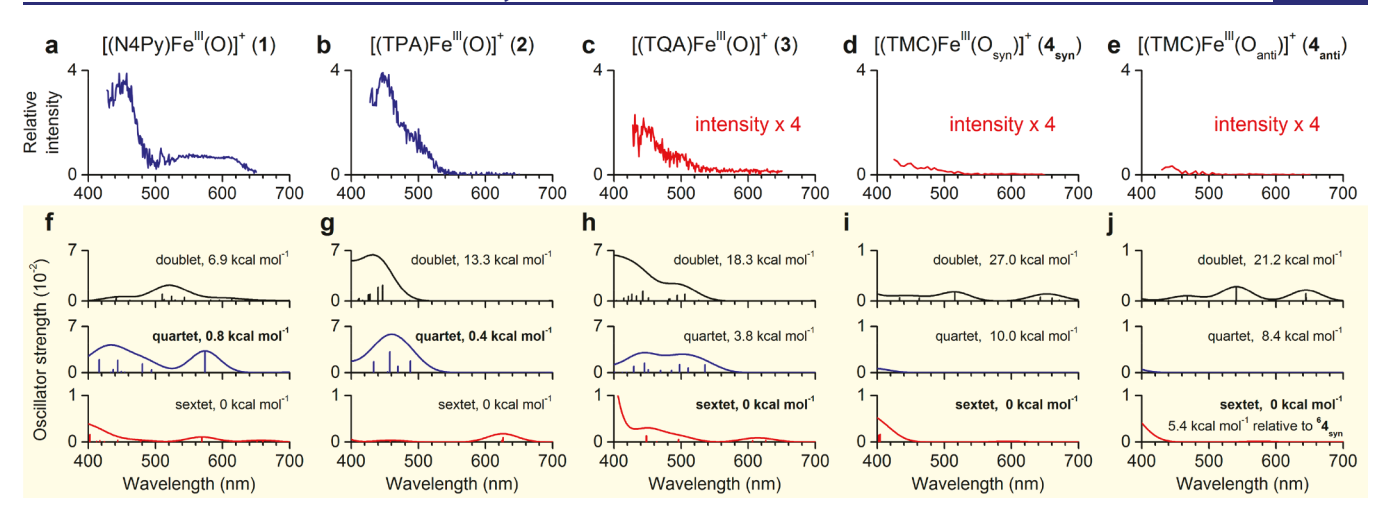


Figure 3. Experimental visible photodissociation spectra of complexes 1–4 measured at 3 K (a–e) and theoretical TD-DFT spectra of complexes 1–4 (f–j). The assigned ground states are highlighted in bold. The relative DFT energies include zero-point energy corrections.

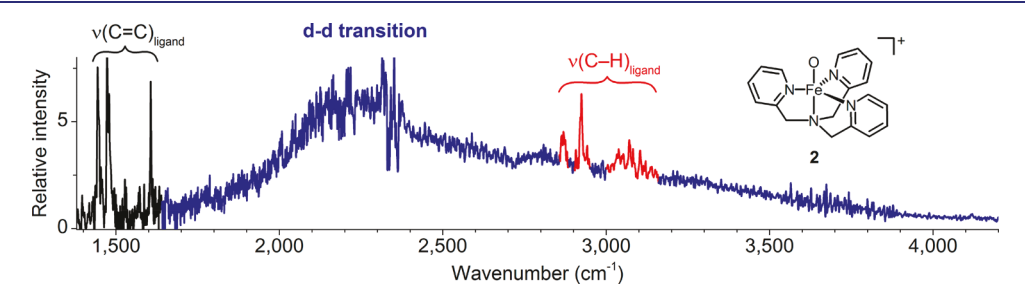


Figure 4. Photodissociation spectrum of 2 measured at 3 K in IR region containing an electronic d-d transition. The spectrum also contains C=C and C-H stretching vibrations of the TPA ligand. The latter vibrations (highlighted in red) are superposed on the electronic absorption band.

vibrations around 1500 cm⁻¹ or C-H stretching vibrations between 2850 and 3150 cm⁻¹. In summary, all experimental data show that the ground state of **2** is also quartet, with the Fe-O band position similar to that in **1**.

In contrast, the Fe-O band of the second trigonal complex $[(TQA)Fe^{III}(O)]^+$ (3) is located at 777 cm⁻¹ (746 cm⁻¹ with ¹⁸O labeling; Figure 1c and Figure S6), showing a decrease in frequency of \sim 75 cm⁻¹ relative to those of 1 and 2. This observation indicates different occupancies of Fe-O antibonding orbitals, thereby suggesting that the ground state of 3 is a sextet state in which all d orbitals, including the Fe-O σ^* antibonding d_{z^2} orbital, are singly occupied (Figure 2b right). Hence, the formal Fe-O bond order in the sextet state decreases to 1.5. We can exclude the doublet state on the basis of DFT calculations, because this state is predicted to be 18.3 kcal mol-1 higher in energy than the sextet state. The sextet ground state assignment also matches the vis spectrum (Figure 3c). First, the absorption intensity of 3 is approximately eight times lower than that of complex 2, which corroborates the theoretical prediction for a sextet state (Figure 3h). Second, the absorption spectrum displays two maxima at 450 and 500 nm and a weak but reproducible broad absorption at longer wavelengths. According to TD-DFT, the observed absorptions correspond to predominantly d-d transitions (Figure S10d), which are spin-forbidden for sextet d⁵ systems and therefore are expected to have particularly low intensity. Hence, the weak intensity of the absorption further supports the assignment of the sextet ground state.

Lastly, we studied the square pyramidal $[(TMC)Fe^{III}(O)]^+$ complexes, which have all four methyl groups either syn (4_{syn})

or anti (4_{anti}) to the oxo ligand, depending on the method of preparation. The syn isomer 4_{syn} was prepared by NO₂ dissociation from [(TMC)Fe^{II}(ONO₂)]⁺ in the gas phase, whereas the *anti* isomer 4_{anti} was formed by one-electron reduction of $[(TMC)Fe^{IV}(O_{anti})(CH_3CN)]^{2+}$ ions in collisions with TDAE in the gas phase (the collisions also triggered the loss of acetonitrile). We anticipated that the vacant axial coordination site in 4 would make the σ^* -antibonding d_z^2 orbital energetically accessible and thus favor the sextet ground state, which should show an Fe-O vibration below 800 cm⁻¹. Indeed, we observed the Fe-O band at 797 cm⁻¹ for 4_{syn} and at 769 cm⁻¹ for 4_{anti} (763 and 732 cm⁻¹ with ¹⁸O labeling, respectively; Figure 1d,e and Figure S7). Accordingly, DFT calculations predict the sextet ground state for 4_{syn} and 4_{anti} , with the quartet and doublet states 10 (8) and 27 (21) kcal mol⁻¹ higher in energy. Furthermore, because the vis spectra of 4_{svn} and 4_{anti} show only very weak absorption (Figure 3d,e), the comparison with the TD-DFT predictions (Figure 3i,j) allows us to exclude the doublet states. Conversely, the predicted vis spectra of the quartet and sextet states are virtually indistinguishable (Figure 3i,j). Therefore, we assign sextet ground states to 4_{syn} and 4_{anti} based on Fe-O frequencies and on relative energetic stabilities, in comparison with other spin states.

The analysis of the iron(III)—oxo complexes in quartet (1, 2) and sextet (3, 4_{syn} , 4_{anti}) states shows that the Fe–O stretching frequency reflects the spin state of the iron(III) center (Table 1). In contrast, our previous results on iron(IV)—oxo complexes showed that Fe–O vibrations are unaffected by their spin state, 53 and similar results were also found in solution. 12,13,15 Interestingly, the Fe–O vibrations of

Table 1. Fe-O Vibrational Frequencies (ν) of Iron(IV)-Oxo and Iron(III)-Oxo Complexes

	$(E_{\bullet}IV \cap O) (-1)a$	$(E_{\alpha}^{\text{III}} \cap (a_{\alpha}))$
	$\nu(\text{Fe}^{\text{IV}}-\text{O}) (\text{cm}^{-1})^a$	$\nu(\text{Fe}^{\text{III}}-\text{O}) (\text{cm}^{-1})^a$
	[18O labeling shift]	[18O labeling shift]
supporting ligand	(spin state)	(spin state)
N4Py (1)	$853 \ [-34]^{53} \ (S=1)$	851 [-36] (S = 3/2)
	$841 [-35]^{19}$	
TPA (2)	$833 \left[-34 \right]^{56} \left(S = 1 \right)^{b}$	856 [-36] (S = 3/2)
TQA (3)	$838 \left[-35 \right]^{36} (S=2)^b$	777 $[-31]$ ($S = 5/2$)
TMC_{syn} (4 _{syn})	$856 \left[-36 \right]^{37} (S = 1)^b$	797 $[-34]$ $(S = 5/2)$
TMC_{anti} (4 _{anti})	$848 \ [-34]^{53} \ (S=1)$	769 [-37] (S = 5/2)
	$834 \ [-34]^{38,b}$	
H ₃ buea	$798 \left[-33 \right]^{57} (S = 2)$	$671 \left[-26\right] \left(S = 5/2\right)^{25}$

^aValues in italics were recorded in solution; spin states are given in parentheses. ^bIn solution, the complex likely has an additional acetonitrile ligand.

the quartet iron(III)-oxo complexes (1, 2) are found at the position typical for iron(IV)-oxo complexes (~850 cm⁻¹), because the fifth d electron is introduced into the $d_{x^2-y^2}$ orbital and does not affect the Fe=O bond order. Therefore, the Fe-O bonds of 1 and 2 have similar strength to those of their iron(IV)-oxo counterparts. In contrast, the Fe-O bonds of the sextet-state complexes 3, 4_{syn}, and 4_{anti} are weakened because the σ^* -antibonding d_{z^2} orbital is occupied. The weaker Fe-O bond translates into the red-shifted Fe-O frequencies of 3, 4_{syn} , and 4_{anti} by $\sim 70 \text{ cm}^{-1}$ relative to those of 1, 2, and iron(IV)-oxo complexes. Nevertheless, the Fe-O frequencies of the sextet complexes 3, 4_{syn} , and 4_{anti} are still blue-shifted by approximately 100 cm⁻¹ in comparison with the Borovik's sextet complex $[(H_3buea)Fe^{III}(O)]^{2-}$ (671 cm⁻¹).²⁵ This substantial shift results from three amide N-H groups of the H₃buea ligand forming hydrogen bonds with the oxo ligand, thus affecting the Fe-O bond properties. So Notably, the Fe-O frequencies roughly correlate with the corresponding Fe-O bond lengths (Figure 5; note that all frequencies are experimental, whereas the bond distances are either experimental or theoretical).

To assess the effect of hydrogen bonding, we prepared complexes of 1, 2, and 3 solvated by a single water molecule in the ion trap of our instrument at 3 K. Figure 6 shows the helium-tagging IRPD spectra of singly hydrated complexes 1. H_2O , $2\cdot H_2O$, and $3\cdot H_2O$. In the case of $4\cdot H_2O$, we were unable to generate a sufficient number of helium-tagged ions to measure the spectrum. We anticipated three possible outcomes for water coordination: (i) The water molecule would not interact with the oxo part of the Fe-O unit (this includes the water coordinated on the iron center). In this case, two free O-H stretching bands of water should be present around 3700 cm⁻¹, and they should not be sensitive to ¹⁸O labeling of the oxo ligand. (ii) The water molecule would form a hydrogen bond with the Fe-O unit (no other hydrogen bond acceptors are present in 1-3). Accordingly, one free O-H vibration of water should be present around 3700 cm⁻¹, which should not respond to ¹⁸O labeling of the oxo ligand. The second O-H vibration should be substantially red-shifted and possibly broadened due to hydrogen bonding, as previously reported for other hydrogen-bound water clusters 59 or metal complexes.⁶⁰ (iii) The water molecule would be deprotonated by the Fe-O unit, yielding the Fe-OH group. Therefore, the remaining hydroxide ion would coordinate to the iron center, thus forming an iron(III)-dihydroxo complex. Consequently,

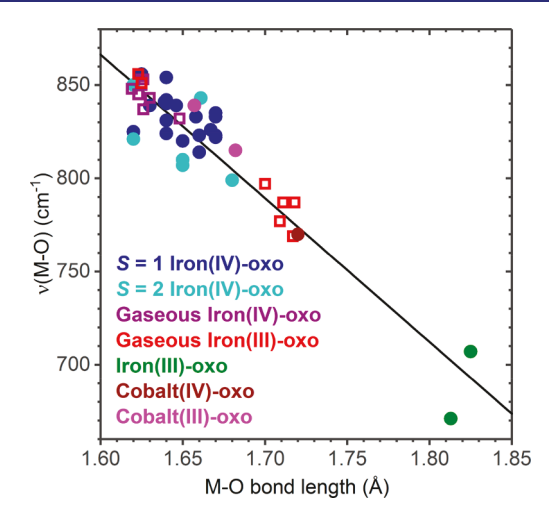


Figure 5. Correlation between the experimental M-O (M = Fe or Co) vibrational frequencies and the experimental (filled circles)/ DFT-calculated (empty squares) M-O bond lengths in M(IV)-oxo and M(III)-oxo complexes (data taken from refs 12, 33, 53, 56, and 58; red squares refer to this study). The linear fit is $\nu(\text{Fe-O}) = 2093$ -766[r(Fe-O)]; $R^2 = 0.88$. More information and the assignment of points to individual complexes can be found in Figure S11 in the Supporting Information.

two free O-H stretches should be present around 3700 cm⁻¹, and one of them should respond to ¹⁸O labeling of the oxo ligand.

The analysis of the spectra in Figure 6, considering the aforementioned possibilities, shows that water forms a hydrogen bond in complexes 1·H₂O and 2·H₂O (Case (ii), Figure 5a,b). The spectra of both complexes contain a band around 3700 cm⁻¹, which does not shift upon ¹⁸O labeling of the oxo ligand. Thus, this band corresponds to a free O-H stretching vibration of the hydrogen-bonded water molecule. Concomitantly, both spectra display a broad absorption between 3200 and 3350 cm⁻¹, which is not present in the spectra of non-hydrated 1 and 2 (Figure 4 and Figure S8). We attribute this broad band to the O-H stretching vibration of the hydrogen-bonded water molecule. Such a red shift in O-H stretching vibration indicates a strong interaction between the water molecule and the iron(III)-oxo complexes 1 and 2.

The hydrogen-bonding interaction with water markedly affects the Fe-O stretching vibration in both complexes 1 and 2. The Fe-O stretching frequency red-shifts from 851 cm⁻¹ in 1 to 787 cm⁻¹ in $1 \cdot H_2O$ ($\Delta = 64$ cm⁻¹, Figure 6a) and from 856 cm⁻¹ in 2 to 787 cm⁻¹ in $2 \cdot H_2O$ ($\Delta = 69 \text{ cm}^{-1}$, Figure 6b). The Fe−O stretching frequencies of 1·H₂O and 2·H₂O fall in the range for sextet complexes 3, 4_{syn}, and 4_{anti}. Moreover, the vis spectrum of 1·H₂O (Figure S9) shows a 20fold decrease in absorption intensity compared with 1. These results suggest a change in the spin state of 1 and 2 upon hydrogen bonding with water. Accordingly, based on our DFT calculations, we predict that the hydrogen bond in 1·H₂O and 2·H₂O stabilizes the sextet over the quartet states, because the hydrogen bond in the sextet states is stronger than in the quartet states by 2.0 kcal mol⁻¹ in 1·H₂O and by 1.9 kcal mol⁻¹ in 2·H₂O. A similar effect of hydrogen bonding on the spin state has been previously reported for an iron(III) porphyrin chlorido complex.⁶¹ Hence, hydrogen bonding changes the spin state of 1 and 2 from quartet to sextet.

The higher stabilization of the sextet states of iron(III)—oxo complexes 1·H₂O and 2·H₂O by hydrogen bonding can be Journal of the American Chemical Society

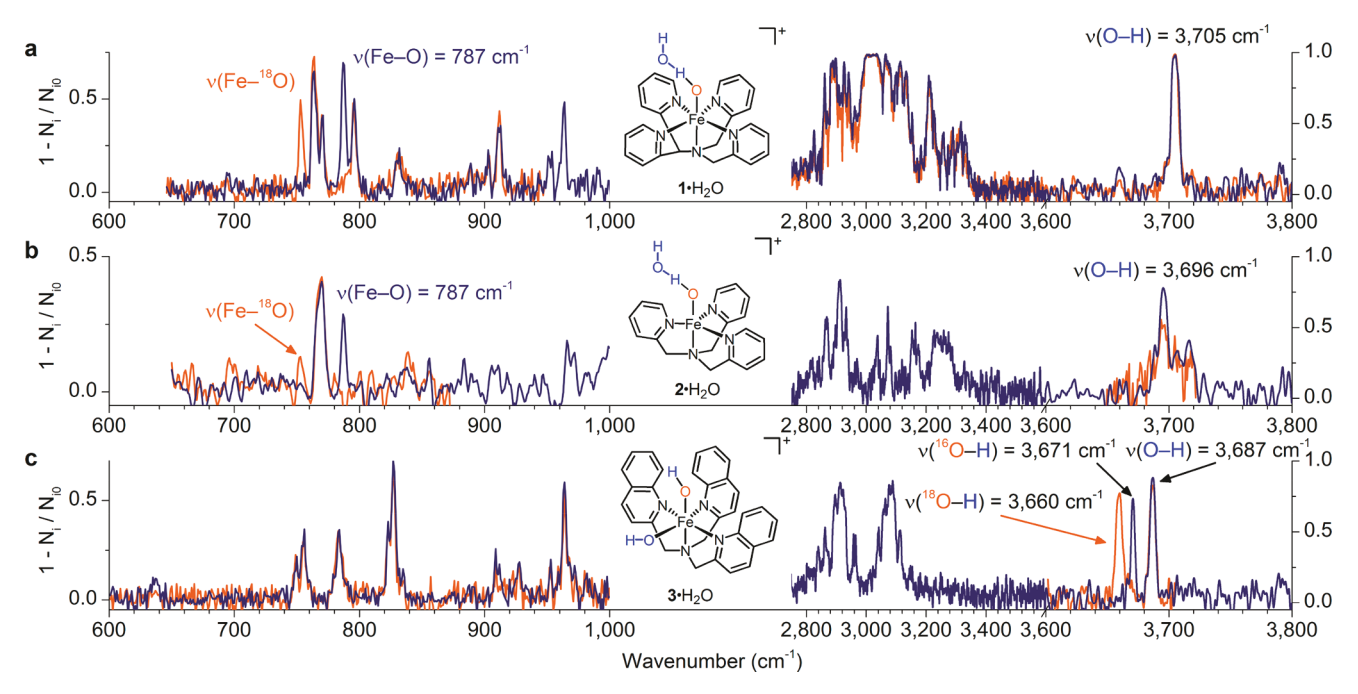


Figure 6. Infrared photodissociation spectra of singly hydrated terminal iron(III)—oxo complexes $1 \cdot H_2O$, $2 \cdot H_2O$, and $3 \cdot H_2O$ measured at 3 K. Blue and orange traces correspond to the ^{16}O and ^{18}O labeling of the oxo ligand, respectively.

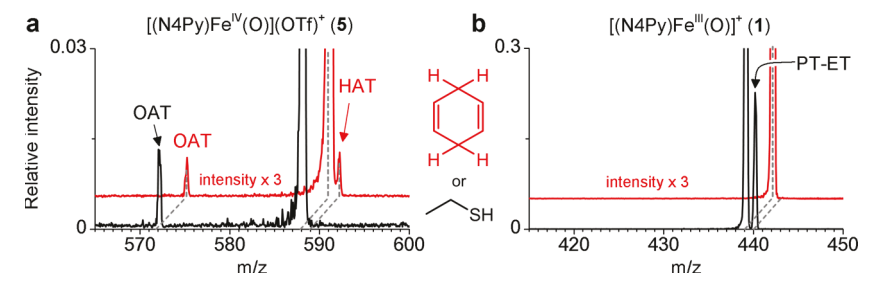


Figure 7. Product mass spectra of gas-phase reactions of iron(IV)—oxo complex 5 (a) and iron(III)—oxo complex 1 (b) with ethanethiol (black traces) and 1,4-cyclohexadiene (red traces) at 0.2 mTorr pressure.

rationalized theoretically.⁶² Natural population analysis⁶³ of 1–4 shows that the Fe–O bond is more polarized (i.e., oxygen carries a larger negative charge) in the sextet than in the quartet states (Table S1). Therefore, the complexes form stronger hydrogen bonds in the sextet states and are more energetically stabilized by hydration than in the quartet states. The difference in stabilization by hydrogen bonding is sufficient to change the ground spin state of 1 and 2 due to small energy differences between the quartet and the sextet states.

Interestingly, the Fe–O frequencies of all sextet complexes (non-hydrated 3, 4_{syn} , and 4_{anti} and hydrated $1 \cdot H_2O$ and $2 \cdot H_2O$) lie within 30 cm⁻¹ of each other. This indicates that the main factor affecting the Fe–O frequency, at least in $1 \cdot H_2O$ and $2 \cdot H_2O$, is the spin state rather than the hydrogen bond itself. Conversely, the presence of three hydrogen bonds and the highly electron-donating ligand plays a key role in further weakening of the Fe–O bond in the sextet $[(H_3buea) \cdot Fe^{III}(O)]^{2-}$ complex, 25,55 which has an Fe–O vibrational frequency of 671 cm⁻¹.

Lastly, the interaction of water with the sextet complex 3 leads to the deprotonation of the water molecule, thus yielding an iron(III)—dihydroxo complex (Case (iii)). The formation of the iron(III)—dihydroxo complex is evidenced by presence

of two free O–H vibrations at 3671 and 3687 cm⁻¹ (Figure 6c). As expected, only one of these O–H bands shifts upon 18 O labeling of the starting iron(III)—oxo complex 3. The experimental 18 O/ 16 O shift (11 cm⁻¹) agrees with the shift predicted for a diatomic oscillator (12 cm⁻¹). Accordingly, no Fe–O stretching vibration is found in the spectrum of $3 \cdot \text{H}_2\text{O}$ (Figure 6c). The Fe–OH vibrations are not present in the spectrum because their frequencies are outside the range of our laser system (<600 cm⁻¹).

We also assessed the effects of water solvation on the iron(IV)-oxo complex $[(N4Py)Fe^{IV}(O)]^{2+}$. The IR spectrum of $[(N4Py)Fe^{IV}(O)]^{2+}\cdot H_2O$ (Figure S8g) contains two free O-H stretching vibrations of water at 3626 cm⁻¹ (symmetric) and 3704 cm⁻¹ (antisymmetric), which are slightly red-shifted compared with the frequencies of a free water molecule (3657 and 3756 cm⁻¹).⁶⁴ However, this shift is typical for a water molecule interacting with a charged species.⁶⁵ Concomitantly, water coordination caused no shift in the Fe=O stretching frequency. Therefore, the water molecule does not interact with the iron(IV)-oxo unit (Case (i)), thus confirming the expected decrease in basicity upon oxidation of the iron(III)-oxo unit. These findings also corroborate previously reported studies on the protonation of iron(IV)-oxo complexes.^{66,67}

Finally, we studied the outcome of one-electron reduction on the hydrogen atom transfer (HAT) reactivity of iron(III)oxo complexes in comparison with their iron(IV)-oxo precursors. Previous studies showed that gaseous iron(IV)oxo complexes react readily with 1,4-cyclohexadiene by HAT from the methylene group (BDE(C-H) 76 kcal mol^{-1}). 40,53,68 Here, for the sake of comparison we show reactivity of $[(N4Py)Fe^{IV}(O)(OTf)]^+$ (5). This iron(IV)—oxo complex bears a loosely bound triflate counterion, which does not affect the iron-oxo moiety, but it makes the complex singly charged and thus directly comparable to 1–4.53 Complex 5 reacts with 1,4-cyclohexadiene by HAT to form a cyclohexadienyl radical or by oxygen atom transfer (OAT) resulting in epoxidation of the C=C bond (Figure 7a, red spectrum). In contrast, studied iron(III)-oxo complexes 1-4 do not react with 1,4-cyclohexadiene at all (Figure 7b, red spectrum; Figure S13). Hence, iron(III)-oxo complexes are inefficient reactants in HAT or OAT reactions.

It is expected that iron(III)—oxo complexes react as bases.⁷⁰ Therefore, we tested their reactivity with acetic acid in the gas phase and observed efficient addition reaction (Figure S12). Presumably, the addition proceeds through a proton transfer followed by association of the resulting dication with acetate anion (eq 3; note that dication-anion separation is not energetically feasible in the gas phase). To gain insight into the mechanism, we investigated the reaction of iron(III)-oxo complexes with ethanethiol. Thiolates undergo electron transfer reactions; 69 therefore, we expected that we might observe proton transfer reaction followed by electron transfer (PT-ET^{70,71} reaction; eq 4). Formally, the PT-ET reaction resembles the hydrogen atom transfer, but the homolytic cleavage of the S-H bond is energetically inaccessible for the studied complexes (BDE(S-H) 87 kcal mol⁻¹ in ethanethiol; thus the S-H bond is stronger than the C-H bond in 1,4cyclohexadiene).72 Instead, we observe the PT-ET reaction for all studied iron(III)-oxo complexes 1-4 (Figure 7b, black spectrum; Figure S13). In comparison, iron(IV)—oxo complex 5 shows no HAT or PT-ET reactivity toward ethanethiol, but only provides OAT to the sulfur atom as expected (Figure 7a, black spectrum). These results demonstrate extraordinary basicity of iron(III)-oxo complexes: despite being positively charged gaseous complexes, they still mediate reactions initiated by their protonation. To the best of our knowledge, this is the first experimental evidence of such a process in the gas phase.

$$[(L)Fe^{III}(O)]^{+} + CH_{3}COOH$$

$$\rightarrow \{[(L)Fe^{III}(OH)]^{2+} \cdot (CH_{3}COO^{-})\}$$

$$\rightarrow [(L)Fe^{III}(OH)(CH_{3}COO)]^{+}$$

$$[(L)Fe^{III}(O)]^{+} + CH_{3}CH_{2}SH$$

$$\rightarrow \{[(L)Fe^{III}(OH)]^{2+} \cdot (CH_{3}CH_{2}S^{-})\}$$

$$\rightarrow [(L)Fe^{II}(OH)]^{+} + CH_{3}CH_{2}S^{-}$$
(4)

The reactions of ethanethiol with 1 and 4_{syn} on one side and with 2 and 3 on the other are different (Figure S13, Table S2). On one hand, we observed the PT-ET mechanism as the dominant pathway in reactions of 1 and 4_{syn} (1 reacts about 100 times faster than 4_{syn}). On the other, the PT-ET pathway is partially suppressed in reactions of 2 and 3 at the expense of the formal addition reaction pathway (proton transfer/

recombination) in analogy with eq 3. Note that the water addition to 3 (discussed above) follows the same pathway, which we also supported by the spectroscopic characterization of the iron(III)-dihydroxo product (Figure 6c). The addition of thiolate is favored over the PT-ET reaction most probably because the complexes 2 and 3 have a vacant coordination site. We also determined KIEs in reactions of 1 and 3 with a mixture of EtSD and EtSH. The KIE of the PT-ET reaction of 1 is 2.1 \pm 0.4. Similarly, KIEs of the PT-ET reaction and the proton transfer/recombination reaction of 3 are 1.7 ± 0.2 and 1.4 ± 0.2 , respectively. The slightly smaller KIE in the proton transfer/recombination reaction pathway can be caused by a partial interference of a direct association reaction (KIE = 1). In comparison, the KIEs observed in HAT reactions of iron(IV)-oxo complexes with 1,4-cyclohexadiene are typically above 3.53 Therefore, the observed KIEs further support the proton transfer (as opposed to HAT) as the rate-limiting step in the studied reactions of iron(III)-oxo complexes with ethanethiol.

CONCLUSION

We have used gas-phase techniques to prepare, for the first time, non-heme terminal iron(III)-oxo complexes with no stabilization from hydrogen bonding and analyze their spectroscopic and chemical properties. The results show that the Fe-O stretching frequencies, and thus the Fe-O bond properties of iron(III)-oxo complexes, are predominantly determined by the spin state of the iron center but not by the symmetry of the supporting ligand. Interestingly, the $\nu(\text{Fe-O})$ frequencies of iron(III)-oxo species 1 and 2 are virtually identical to those of the corresponding triplet iron(IV)-oxo complexes, showing that the Fe=O bond order of 2 is maintained upon one-electron reduction and indicating that the introduced electron occupies an antibonding orbital with hardly any Fe=O bonding character. These results are best rationalized by assigning quartet spin states to 1 and 2. Conversely, 3, 4_{syn} , and 4_{anti} exhibit $\nu(\text{Fe-O})$ frequencies 60– 80 cm⁻¹ lower, reflecting a decreased Fe=O bond order and a change to the sextet spin state. In turn, due to the presence of hydrogen-bonding interactions, the Borovik's sextet-state iron(III)-oxo complex has an even lower $\nu(\text{Fe-O})$ at 671 cm⁻¹, which is comparable to that of the sextet-state complex $[(N4Py)Fe^{III}-O-Ce^{IV}(NO_3)_4(H_2O)]^+$ (707 cm⁻¹) with a Ce(IV) ion replacing the three hydrogen bonds.⁷

Our study also show that the coordination of a single water molecule to the iron(III)—oxo complexes affects their ν (Fe—O) frequencies. In quartet state complexes 1 and 2, the water molecule forms a strong hydrogen bond with the oxo ligand and triggers the change from the quartet to the sextet ground spin state. Experimentally, this change is reflected by a red shift of ~70 cm⁻¹ in the ν (Fe—O) frequency. In contrast, the sextet-state complex 3 reacts with water and forms the iron(III)—dihydroxo complex. On the other hand, the singly hydrated iron(IV)—oxo complex $[(N4Py)Fe^{IV}(O)]^{2+}\cdot H_2O$ has an unperturbed Fe—O vibrational frequency, which shows that the water molecule forms no hydrogen bond with the iron(IV)—oxo unit, thus reflecting the poor nucleophilicity of this iron(IV)—oxo unit.

We have studied the reactivity of iron(III)—oxo complexes and demonstrated their extraordinary basicity. The positively charged gaseous iron(III)—oxo complexes are capable of initiating the reaction with ethanethiol by proton abstraction.

The proton transfer is followed by either electron transfer or recombination between the nascent dication and the anion.

Our results also shed light on the electronic structure of the isoelectronic $[(13\text{-}TMC)Co^{IV}(O)]^{2+}$ complex recently reported by Wang et al.³³ This complex exhibits the $\nu(\text{Co-O}) = 770 \text{ cm}^{-1}$, which is remarkably similar to our $\nu(\text{Fe-O})$ data on the sextet spin state iron(III)—oxo species 3, 4_{syn} , and $4_{\text{anti-Therefore}}$, we suggest also assigning the sextet spin state to the $[(13\text{-}TMC)Co^{IV}(O)]^{2+}$ complex, which is consistent with its reported EPR signals of $g_{\perp} = 6.5$ and $g_{\parallel} = 2.02$ and its longer Co-O bond length of 1.72 Å obtained by EXAFS analysis (Figure S11).

Thus, we have described the gas-phase preparation and properties of several iron(III)—oxo species in trigonal and tetragonal ligand environments without stabilization by hydrogen bonds. These complexes represent examples of first row metal—oxo species with five d electrons at the boundary of the "Oxo Wall".

ASSOCIATED CONTENT

S Supporting Information

The Supporting Information is available free of charge on the ACS Publications website at DOI: 10.1021/jacs.8b08950.

Preparation of ¹⁸O-labeled nitric acid, Tables S1 and S2, Figures S1–S14, and XYZ coordinates of calculated structures (PDF)

AUTHOR INFORMATION

Corresponding Authors

- *jana.roithova@ru.nl
- *larryque@umn.edu
- *miquel.costas@udg.edu

ORCID ®

Erik Andris: 0000-0002-9336-0157 Miquel Costas: 0000-0001-6326-8299 Lawrence Que, Jr.: 0000-0002-0989-2813 Jana Roithová: 0000-0001-5144-0688

Author Contributions

¹E.A. and R.N. contributed equally to this work.

Notes

The authors declare no competing financial interest.

ACKNOWLEDGMENTS

The project was funded by the European Research Council (ERC CoG No. 682275), the Czech Ministry of Education, Youth and Sports (LTAUSA17026) and the COST action ECOSTBio. MC acknowledges the financial support from the MINECO of Spain (CTQ2015-70795-P), the Catalan DIUE of the Generalitat de Catalunya (2009SGR637) and the ICREA-Academia award. MP acknowledges a doctoral dissertation fellowship from the University of Minnesota and LQ thanks the US National Science Foundation for support (CHE1665391). The authors would like to thank Dr. Carlos V. Melo for proofreading the manuscript.

REFERENCES

(1) Costas, M.; Mehn, M. P.; Jensen, M. P.; Que, L., Jr. Oxygen Activation at Mononuclear Nonheme Iron: Enzymes, Intermediates, and Models. *Chem. Rev.* **2004**, *104*, 939–986.

- (2) Stone, K. L.; Borovik, A. S. Lessons from nature: unraveling biological C-H bond activation. *Curr. Opin. Chem. Biol.* **2009**, *13*, 114–118.
- (3) Solomon, E. I.; Light, K. M.; Liu, L. V.; Srnec, M.; Wong, S. D. Geometric and Electronic Structure Contributions to Function in Non-heme Iron Enzymes. *Acc. Chem. Res.* **2013**, *46*, 2725–2739.
- (4) Iron Containing Enzymes: Versatile Catalysts of Hydroxylation Reactions in Nature; de Visser, S. P., Kumar, D., Eds.; RSC Publishing: Cambridge, UK, 2011.
- (5) Company, A., Lloret-Fillol, J., Costas, M. Small Molecule Models for Nonporphyrinic Iron and Manganese Oxygenases. In *Comprehensive Inorganic Chemistry II*; Reedijk, J., Poeppelmeier, K., Eds.; Elsevier: Oxford, 2013; Vol. 3, pp 487–564.
- (6) Price, J. C.; Barr, E. W.; Tirupati, B.; Bollinger, J. M., Jr.; Krebs, C. The First Direct Characterization of a High-Valent Iron Intermediate in the Reaction of an α -Ketoglutarate-Dependent Dioxygenase: A High-Spin Fe(IV) Complex in Taurine/ α -Ketoglutarate Dioxygenase (TauD) from *Escherichia coli. Biochemistry* **2003**, 42, 7497–7508.
- (7) Bollinger, J. M., Jr.; Krebs, C. Stalking intermediates in oxygen activation by iron enzymes: motivation and method. *J. Inorg. Biochem.* **2006**, *100*, 586–605.
- (8) Krebs, C.; Galonić Fujimori, D.; Walsh, C. T.; Bollinger, J. M., Jr. Non-Heme Fe(IV)—Oxo Intermediates. *Acc. Chem. Res.* **2007**, *40*, 484—492.
- (9) Engelmann, X.; Monte-Perez, I.; Ray, K. Oxidation Reactions with Bioinspired Mononuclear Non-Heme Metal—Oxo Complexes. *Angew. Chem., Int. Ed.* **2016**, *55*, 7632–7649.
- (10) Abu-Omar, M. M.; Loaiza, A.; Hontzeas, N. Reaction Mechanisms of Mononuclear Non-Heme Iron Oxygenases. *Chem. Rev.* **2005**, *105*, 2227–2252.
- (11) Meunier, B.; de Visser, S. P.; Shaik, S. Mechanism of Oxidation Reactions Catalyzed by Cytochrome P450 Enzymes. *Chem. Rev.* **2004**, 104, 3947–3980.
- (12) Klein, J. E. M. N.; Que, L., Jr. Biomimetic High-Valent Mononuclear Nonheme Iron-Oxo Chemistry. In *Encyclopedia of Inorganic and Bioinorganic Chemistry*; Scott, R. A., Ed.; John Wiley: Chichester, UK, 2016; DOI: 10.1002/9781119951438.eibc2344.
- (13) Hohenberger, J.; Ray, K.; Meyer, K. The biology and chemistry of high-valent iron—oxo and iron—nitrido complexes. *Nat. Commun.* **2012**, *3*, 720.
- (14) Ray, K.; Pfaff, F. F.; Wang, B.; Nam, W. Status of Reactive Non-Heme Metal—Oxygen Intermediates in Chemical and Enzymatic Reactions. *J. Am. Chem. Soc.* **2014**, *136*, 13942—13958.
- (15) McDonald, A. R.; Que, L., Jr. High-valent nonheme iron-oxo complexes: Synthesis, structure, and spectroscopy. *Coord. Chem. Rev.* **2013**, 257, 414–428.
- (16) Mayer, J. M. Proton-Coupled Electron Transfer: A Reaction Chemist's View. *Annu. Rev. Phys. Chem.* **2004**, *55*, 363–390.
- (17) Fukuzumi, S. Electron-transfer properties of high-valent metaloxo complexes. *Coord. Chem. Rev.* **2013**, 257, 1564–1575.
- (18) Sastri, C. V.; Lee, J.; Oh, K.; Lee, Y. J.; Lee, J.; Jackson, T. A.; Ray, K.; Hirao, H.; Shin, W.; Halfen, J. A.; Kim, J.; Que, L., Jr.; Shaik, S.; Nam, W. Axial ligand tuning of a nonheme iron(IV)—oxo unit for hydrogen atom abstraction. *Proc. Natl. Acad. Sci. U. S. A.* **2007**, *104*, 19181—19186.
- (19) Wang, D.; Ray, K.; Collins, M. J.; Farquhar, E. R.; Frisch, J. R.; Gomez, L.; Jackson, T. A.; Kerscher, M.; Waleska, A.; Comba, P.; Costas, M.; Que, L., Jr. Nonheme oxoiron(IV) complexes of pentadentate N5 ligands: spectroscopy, electrochemistry, and oxidative reactivity. *Chem. Sci.* 2013, 4, 282–291.
- (20) Lee, Y.-M.; Kotani, H.; Suenobu, T.; Nam, W.; Fukuzumi, S. Fundamental Electron-Transfer Properties of Non-heme Oxoiron(IV) Complexes. J. Am. Chem. Soc. 2008, 130, 434–435.
- (21) Nam, W.; Lee, Y.-M.; Fukuzumi, S. Tuning Reactivity and Mechanism in Oxidation Reactions by Mononuclear Nonheme Iron(IV)-Oxo Complexes. *Acc. Chem. Res.* **2014**, *47*, 1146–1154.

- (22) Nehru, K.; Seo, M. S.; Kim, J.; Nam, W. Oxidative N-Dealkylation Reactions by Oxoiron(IV) Complexes of Nonheme and Heme Ligands. *Inorg. Chem.* **2007**, *46*, 293–298.
- (23) de Visser, S. P.; Oh, K.; Han, A.-R.; Nam, W. Combined Experimental and Theoretical Study on Aromatic Hydroxylation by Mononuclear Nonheme Iron(IV)—Oxo Complexes. *Inorg. Chem.* **2007**, *46*, 4632–4641.
- (24) Morimoto, Y.; Park, J.; Suenobu, T.; Lee, Y.-M.; Nam, W.; Fukuzumi, S. Mechanistic Borderline of One-Step Hydrogen Atom Transfer versus Stepwise Sc³⁺-Coupled Electron Transfer from Benzyl Alcohol Derivatives to a Non-Heme Iron(IV)-Oxo Complex. *Inorg. Chem.* **2012**, *51*, 10025–10036.
- (25) MacBeth, C. E.; Golombek, A. P.; Young, V. G.; Yang, C.; Kuczera, K.; Hendrich, M. P.; Borovik, A. S. O₂ Activation by Nonheme Iron Complexes: A Monomeric Fe(III)-Oxo Complex Derived From O₂. *Science* **2000**, 289, 938–941.
- (26) Matson, E. M.; Park, Y. J.; Fout, A. R. Facile Nitrite Reduction in a Non-heme Iron System: Formation of an Iron(III)-Oxo. *J. Am. Chem. Soc.* **2014**, *136*, 17398–17401.
- (27) Cook, S. A.; Borovik, A. S. Molecular Designs for Controlling the Local Environments around Metal Ions. *Acc. Chem. Res.* **2015**, *48*, 2407–2414.
- (28) Gray, H. B.; Winkler, J. R. Living with Oxygen. Acc. Chem. Res. **2018**, *51*, 1850–1857.
- (29) Winkler, J. R.; Gray, H. B. Electronic Structures of Oxo-Metal Ions. Struct. Bonding (Berlin, Ger.) 2011, 142, 17–28.
- (30) Holm, R. H. Metal-Centered Oxygen Atom Transfer Reactions. *Chem. Rev.* **1987**, *87*, 1401–1449.
- (31) O'Halloran, K. P.; Zhao, C.; Ando, N. S.; Schultz, A. J.; Koetzle, T. F.; Piccoli, P. M. B.; Hedman, B.; Hodgson, K. O.; Bobyr, E.; Kirk, M. L.; Knottenbelt, S.; Depperman, E. C.; Stein, B.; Anderson, T. M.; Cao, R.; Geletii, Y. V.; Hardcastle, K. I.; Musaev, D. G.; Neiwert, W. A.; Fang, X.; Morokuma, K.; Wu, S.; Kogerler, P.; Hill, C. L. Revisiting the Polyoxometalate-Based Late-Transition-Metal-Oxo Complexes: The "Oxo Wall" Stands. *Inorg. Chem.* **2012**, *51*, 7025–7031.
- (32) Ray, K.; Heims, F.; Pfaff, F. F. Terminal Oxo and Imido Transition-Metal Complexes of Groups 9–11. Eur. J. Inorg. Chem. 2013, 2013, 3784–3807.
- (33) Wang, B.; Lee, Y.-M.; Tcho, W.-Y.; Tussupbayev, S.; Kim, S.-T.; Kim, Y.; Seo, M. S.; Cho, K.-B.; Dede, Y.; Keegan, B. C.; Ogura, T.; Kim, S. H.; Ohta, T.; Baik, M.-H.; Ray, K.; Shearer, J.; Nam, W. Synthesis and reactivity of a mononuclear non-haem cobalt(IV)-oxo complex. *Nat. Commun.* 2017, *8*, 14839.
- (34) Lubben, M.; Meetsma, A.; Wilkinson, E. C.; Feringa, B.; Que, L., Jr. Nonheme Iron Centers in Oxygen Activation: Characterization of an Iron(III) Hydroperoxide Intermediate. *Angew. Chem., Int. Ed. Engl.* **1995**, 34, 1512–1514.
- (35) Lim, M. H.; Rohde, J. U.; Stubna, A.; Bukowski, M. R.; Costas, M.; Ho, R. Y. N.; Münck, E.; Nam, W.; Que, L., Jr. An Fe^W=O complex of a tetradentate tripodal nonheme ligand. *Proc. Natl. Acad. Sci. U. S. A.* **2003**, *100*, 3665–3670.
- (36) Biswas, A. N.; Puri, M.; Meier, K. K.; Oloo, W. N.; Rohde, G. T.; Bominaar, E. L.; Münck, E.; Que, L., Jr. Modeling TauD-J: A High-Spin Nonheme Oxoiron(IV) Complex with High Reactivity toward C–H Bonds. J. Am. Chem. Soc. 2015, 137, 2428–2431.
- (37) Prakash, J.; Rohde, G. T.; Meier, K. K.; Münck, E.; Que, L., Jr. Upside Down! Crystallographic and Spectroscopic Characterization of an [Fe^{IV}(O_{syn})(TMC)]²⁺ Complex. *Inorg. Chem.* **2015**, *54*, 11055–11057.
- (38) Rohde, J.-U.; In, J.-H.; Lim, M. H.; Brennessel, W. W.; Bukowski, M. R.; Stubna, A.; Münck, E.; Nam, W.; Que, L., Jr. Crystallographic and Spectroscopic Characterization of a Nonheme Fe(IV)=O Complex. *Science* **2003**, 299, 1037–1039.
- (39) Schröder, D.; Roithová, J.; Schwarz, H. Electrospray ionization as a convenient new method for the generation of catalytically active iron-oxide ions in the gas phase. *Int. J. Mass Spectrom.* **2006**, 254, 197–201.

- (40) Andris, E.; Jašík, J.; Gómez, L.; Costas, M.; Roithová, J. Spectroscopic Characterization and Reactivity of Triplet and Quintet Iron(IV) Oxo Complexes in the Gas Phase. *Angew. Chem., Int. Ed.* **2016**, *55*, 3637–3641.
- (41) Anbar, M.; Guttmann, S. The Catalytic Effect of Chloride Ions on the Isotopic Oxygen Exchange of Nitric and Bromic Acids with Water. J. Am. Chem. Soc. 1961, 83, 4741–4745.
- (42) Jašík, J.; Žabka, J.; Roithová, J.; Gerlich, D. Infrared spectroscopy of trapped molecular dications below 4 K. *Int. J. Mass Spectrom.* **2013**, 354–355, 204–210.
- (43) Jašík, J.; Navrátil, R.; Němec, I.; Roithová, J. Infrared and Visible Photodissociation Spectra of Rhodamine Ions at 3 K in the Gas Phase. *J. Phys. Chem. A* **2015**, *119*, 12648–12655.
- (44) Roithová, J.; Gray, A.; Andris, E.; Jašík, J.; Gerlich, D. Helium Tagging Infrared Photodissociation Spectroscopy of Reactive Ions. *Acc. Chem. Res.* **2016**, *49*, 223–230.
- (45) Ducháčková, L.; Roithová, J. The Interaction of Zinc(II) and Hydroxamic Acids and a Metal-Triggered Lossen Rearrangement. *Chem. Eur. J.* **2009**, *15*, 13399–13405.
- (46) Jašíková, L.; Roithová, J. Interaction of the Gold(I) Cation Au(PMe₃)⁺ with Unsaturated Hydrocarbons. *Organometallics* **2012**, 31, 1935–1942.
- (47) Becke, A. D. Density-functional thermochemistry. III. The role of exact exchange. *J. Chem. Phys.* **1993**, *98*, 5648–5652.
- (48) Lee, C.; Yang, W.; Parr, R. G. Development of the Colle-Salvetti correlation-energy formula into a functional of the electron density. *Phys. Rev. B: Condens. Matter Mater. Phys.* **1988**, 37, 785–789.
- (49) Miehlich, B.; Savin, A.; Stoll, H.; Preuss, H. Results obtained with the correlation-energy density functionals of Becke and Lee, Yang and Parr. *Chem. Phys. Lett.* **1989**, *157*, 200–206.
- (50) Stephens, P. J.; Devlin, F. J.; Chabalowski, C. F.; Frisch, M. J. *Ab Initio* Calculation of Vibrational Absorption and Circular Dichroism Spectra Using Density Functional Force Fields. *J. Phys. Chem.* **1994**, *98*, 11623–11627.
- (51) Grimme, S.; Antony, J.; Ehrlich, S.; Krieg, H. A consistent and accurate *ab initio* parametrization of density functional dispersion correction (DFT-D) for the 94 elements H-Pu. *J. Chem. Phys.* **2010**, 132. 154104.
- (52) Frisch, M. J.; Trucks, G. W.; Schlegel, H. B.; Scuseria, G. E.; Robb, M. A.; Cheeseman, J. R.; Scalmani, G.; Barone, V.; Mennucci, B.; Petersson, G. A.; Nakatsuji, H.; Caricato, M.; Li, X.; Hratchian, H. P.; Izmaylov, A. F.; Bloino, J.; Zheng, G.; Sonnenberg, J. L.; Hada, M.; Ehara, M.; Toyota, K.; Fukuda, R.; Hasegawa, J.; Ishida, M.; Nakajima, T.; Honda, Y.; Kitao, O.; Nakai, H.; Vreven, T.; Montgomery, J. A., Jr.; Peralta, J. E.; Ogliaro, F.; Bearpark, M.; Heyd, J. J.; Brothers, E.; Kudin, K. N.; Staroverov, V. N.; Keith, T.; Kobayashi, R.; Normand, J.; Raghavachari, K.; Rendell, A.; Burant, J. C.; Iyengar, S. S.; Tomasi, J.; Cossi, M.; Rega, N.; Millam, J. M.; Klene, M.; Knox, J. E.; Cross, J. B.; Bakken, V.; Adamo, C.; Jaramillo, J.; Gomperts, R.; Stratmann, R. E.; Yazyev, O.; Austin, A. J.; Cammi, R.; Pomelli, C.; Ochterski, J. W.; Martin, R. L.; Morokuma, K.; Zakrzewski, V. G.; Voth, G. A.; Salvador, P.; Dannenberg, J. J.; Dapprich, S.; Daniels, A. D.; Farkas, O.; Foresman, J. B.; Ortiz, J. V.; Cioslowski, J.; Fox, D. J. Gaussian 09, revision D.01; Gaussian, Inc.: Wallingford, CT, 2013.
- (53) Andris, E.; Navrátil, R.; Jašík, J.; Terencio, T.; Srnec, M.; Costas, M.; Roithová, J. Chasing the Evasive Fe=O Stretch and the Spin State of the Iron(IV)—Oxo Complexes by Photodissociation Spectroscopy. J. Am. Chem. Soc. 2017, 139, 2757–2765.
- (54) TD-DFT calculations also predicted the other quartet state complex 1 to feature a similar d-d transition located at 10 800 cm⁻¹ (920 nm). However, this frequency range is not accessible with our current laser setup, even if we consider the inaccuracy of TD-DFT prediction.
- (55) Budria, J. G.; Raugei, S.; Cavallo, L. Structure and Bonding in Monomeric Iron(III) Complexes with Terminal Oxo and Hydroxo Ligands. *Inorg. Chem.* **2006**, *45*, 1732–1738.

- (56) Frisch, J. R. Spectroscopic and crystallographic characterization of peroxo- and oxoiron complexes. Ph.D. Dissertation, University of Minnesota, 2010.
- (57) Lacy, D. C.; Gupta, R.; Stone, K. L.; Greaves, J.; Ziller, J. W.; Hendrich, M. P.; Borovik, A. S. Formation, Structure, and EPR Detection of a High Spin Fe^{IV}-Oxo Species Derived from Either an Fe^{III}-Oxo or Fe^{III}-OH Complex. *J. Am. Chem. Soc.* **2010**, *132*, 12188–12190.
- (58) Goetz, M. K.; Hill, E. A.; Filatov, A. S.; Anderson, J. S. Isolation of a Terminal Co(III)-Oxo Complex. *J. Am. Chem. Soc.* **2018**, DOI: 10.1021/jacs.8b07399.
- (59) Shin, J. W.; Hammer, N. I.; Diken, E. G.; Johnson, M. A.; Walters, R. S.; Jaeger, T. D.; Duncan, M. A.; Christie, R. A.; Jordan, K. D. Infrared signature of structures associated with the $H^+(H_2O)_n$ (n = 6 to 27) clusters. *Science* **2004**, 304, 1137–1140.
- (60) Duffy, E. M.; Marsh, B. M.; Garand, E. Probing the Hydrogen-Bonded Water Network at the Active Site of a Water Oxidation Catalyst: [Ru(bpy)(tpy)(H₂O)]²⁺·(H₂O)₀₋₄. *J. Phys. Chem. A* **2015**, 119, 6326–6332.
- (61) Sahoo, D.; Quesne, M. G.; de Visser, S. P.; Rath, S. P. Hydrogen-Bonding Interactions Trigger a Spin-Flip in Iron(III) Porphyrin Complexes. *Angew. Chem.* **2015**, 127, 4878–4882.
- (62) Dey, A.; Hocking, R. K.; Larsen, P.; Borovik, A. S.; Hodgson, K. O.; Hedman, B.; Solomon, E. I. X-ray Absorption Spectroscopy and Density Functional Theory Studies of [(H₃buea)Fe^{III-}X]ⁿ⁻ (X = S²⁻, O²⁻, OH⁻): Comparison of Bonding and Hydrogen Bonding in Oxo and Sulfido Complexes. *J. Am. Chem. Soc.* **2006**, *128*, 9825–9833.
- (63) Reed, A. E.; Weinstock, R. B.; Weinhold, F. Natural population analysis. *J. Chem. Phys.* **1985**, 83, 735–746.
- (64) Shimanouchi, T. Molecular Vibrational Frequencies. In NIST Chemistry WebBook, NIST Standard Reference Database Number 69; Linstrom, P. J., Mallard, W. G., Eds.; National Institute of Standards and Technology: Gaithersburg, MD.
- (65) O'Brien, J. T.; Williams, E. R. Coordination Numbers of Hydrated Divalent Transition Metal Ions Investigated with IRPD Spectroscopy. *J. Phys. Chem. A* **2011**, *115*, 14612–14619.
- (66) Casadei, C. M.; Gumiero, A.; Metcalfe, C. L.; Murphy, E. J.; Basran, J.; Concilio, M. G.; Teixeira, S. C.; Schrader, T. E.; Fielding, A. J.; Ostermann, A.; Blakeley, M. P.; Raven, E. L.; Moody, P. C. Heme enzymes. Neutron cryo-crystallography captures the protonation state of ferryl heme in a peroxidase. *Science* **2014**, *345*, 193–197.
- (67) Fukuzumi, S.; Kotani, H.; Lee, Y.-M.; Nam, W. Sequential Electron-Transfer and Proton-Transfer Pathways in Hydride-Transfer Reactions from Dihydronicotinamide Adenine Dinucleotide Analogues to Non-heme Oxoiron(IV) Complexes and p-Chloranil. Detection of Radical Cations of NADH Analogues in Acid-Promoted Hydride-Transfer Reactions. *J. Am. Chem. Soc.* **2008**, *130*, 15134–15142.
- (68) Tsang, W. Thermodynamic and kinetic properties of the cyclohexadienyl radical. *J. Phys. Chem.* **1986**, *90*, 1152–1155.
- (69) Trujillo, M.; Alvarez, B.; Radi, R. One- and two-electron oxidation of thiols: mechanisms, kinetics and biological fates. *Free Radical Res.* **2016**, *50*, 150–171.
- (70) Weinberg, D. R.; Gagliardi, C. J.; Hull, J. F.; Fecenko Murphy, C.; Kent, C. A.; Westlake, B. C.; Paul, A.; Ess, D. H.; Granville McCafferty, D.; Meyer, T. J. Proton-Coupled Electron Transfer. *Chem. Rev.* **2012**, *112*, 4016–4093.
- (71) Usharani, D.; Lacy, D. C.; Borovik, A. S.; Shaik, S. Dichotomous Hydrogen Atom Transfer vs Proton-Coupled Electron Transfer During Activation of X–H Bonds (X = C, N, O) by Nonheme Iron–Oxo Complexes of Variable Basicity. *J. Am. Chem. Soc.* **2013**, *135*, 17090–17104.
- (72) Janousek, B. K.; Reed, K. J.; Brauman, J. I. Electron photodetachment from mercaptyl anions (RS⁻ electron affinities of mercaptyl radicals and the S-H bond strength in mercaptans). *J. Am. Chem. Soc.* **1980**, *102*, 3125–3129.
- (73) The groups of Schwarz and Shaik proposed a proton-coupled electron-transfer (PCET) mechanism for the reaction between

- gaseous $Al_2O_2^+$ and methane: Li, J.; Zhou, S.; Zhang, J.; Schlangen, M.; Weiske, T.; Usharani, D.; Shaik, S.; Schwarz, H. J. Am. Chem. Soc. **2016**, 138, 7973–7981. Our report is, however, the first one showing a distinct reactivity difference in formal gaseous HAT reactions with nonpolar and polar X–H bonds.
- (74) Draksharapu, A.; Rasheed, W.; Klein, J. E. M. N.; Que, L., Jr. Facile and Reversible Formation of Iron(III)—Oxo—Cerium(IV) Adducts from Nonheme Oxoiron(IV) Complexes and Cerium(III). *Angew. Chem., Int. Ed.* **2017**, *56*, 9091—9095.